



Case Study

Identification of cinnabar existing in different objects using portable coupled XRF-XRD, laboratory-type XRD and micro-Raman spectroscopy: comparison of the techniques

Jingyi Shen¹ · Yijia Shen¹

Received: 24 May 2021 / Accepted: 2 November 2021

Published online: 14 November 2021

© The Author(s) 2021 [OPEN](#)

Abstract

Cinnabar (α -HgS) is a common mineral used in various fields. The identification of cinnabar can be achieved by classic mineralogical methods and instrumental methods. X-ray diffraction (XRD) is the most reliable instrumental method for identifying material phases, but the sampling process and the immovable instrument limit its wider application in the cultural heritage field. The occurrence of Assing S. p. A. Surface Monitor, a portable system integrating X-ray fluorescence (XRF) and XRD, provides researchers with a new solution. Raw mineral, polished gemstone, pigment powder and Chinese ink stick claimed to be composed of cinnabar were measured by the system as well as laboratory-type XRD and micro-Raman techniques in this study. The qualitative XRF results were applied to determining the elements existing in the samples and thus defining the range of possible phases. Patterns obtained were compared carefully with the characteristic lines to determine the most likely phases, while the pattern appearances were compared in order to recognize the different states of cinnabar and generalize the experience for identifying cinnabar by the system. The Raman spectra obtained were compared and analyzed in order to learn the best parameters and determine the real composition of each sample. The results indicate that the XRF detector is sensitive enough to distinguish cinnabar from another red pigment, minium (Pb_3O_4), without destructive preparation provided that the desired phases occupy a major content in the sample, while the laser micro-Raman is even better in application range and measurement speed but correct analysis of the spectra is highly dependent on experience and literatures. The portable coupled XRF-XRD system and the micro-Raman provide researchers with convenient and efficient options to preliminarily identify minerals like cinnabar, which is significantly meaningful to several research fields including mineralogy, heritage science, material science, etc.

Article highlights

- Two efficient and non-destructive methods for the preliminary identification of minerals like cinnabar were developed.
- The optimum instrument parameters for the effective measurement of different cinnabar samples were given in detail.
- The study provides useful data for various fields including analytical science, material science, heritage science, etc.

Keywords Cinnabar · Mineralogy · X-ray diffraction · Raman spectroscopy · Cultural heritage · Portable apparatus · Instrumental analysis

✉ Jingyi Shen, shenjingyi1983@126.com | ¹Shanghai Museum Conservation Center, Shanghai Museum, Shanghai 200231, China.



SN Applied Sciences

(2021) 3:866

| <https://doi.org/10.1007/s42452-021-04858-0>

SN Applied Sciences
A **SPRINGER NATURE** journal

1 Introduction

Originated from volcanic activity [1], cinnabar (α -HgS) is commonly used in various fields such as metallurgy [2] and medicine [3]. Cinnabar is concerned by archaeometry because it was commonly applied to producing the red color on ancient objects [4, 5]. Pure bulky cinnabar crystals, or cinnabar-containing minerals of special shape or pattern, are even regarded as gems. Therefore, it is meaningful for curators to develop simple and effective methods to identify cinnabar in various objects. Classic mineralogical methods and instrumental methods are efficient in identifying cinnabar under normal conditions, but the special requirements in the cultural heritage field such as simple, non-destructive and field inspection should also be considered. Powder X-ray diffraction (XRD) is the most reliable instrumental method for identifying material phases [6], but its application in the cultural heritage field is limited due to the sampling process and the immovable instrument. One promising solution is the Assing S. p. A. (Italy) Surface Monitor, a portable system integrating X-ray fluorescence (XRF) and XRD, which not only meets the above requirements, but also features the phase identification assisted by the simultaneous element detection. The system has been typically applied to the identification of pigments used on ancient Roman frescoes [7] and Renaissance oil paintings [8], but the identification of phases in other objects has not been recognized adequately.

Raman spectroscopy is useful in phase identification due to some advantages like quick measurement, low sample content and high sensitivity, which make it appreciated in some special application scenarios [9]. For example, Raman spectroscopy is widely applied to identifying special samples, such as gems [9, 10], precious traditional herbs [11] and cultural objects [12–14]. The Raman technique is regarded as non-destructive provided that appropriate working modes and parameters are adopted. Compared with XRD and infrared methods, however, Raman is weak in the scale of standard spectra database, the difficulty of spectra analysis, and the availability of instruments [15]. As for the curators, Raman spectroscopy is an ideal non-destructive method for the identification of unknown pigments, minerals, patinas, etc., provided that the key instrumental parameters for the similar objects have been determined and the differences between similar objects have been considered carefully. Therefore, accumulation and analysis of Raman data is an important and constant work of museum researchers.

Raw mineral, polished gemstone, pigment powder and Chinese ink stick claimed to be composed of

cinnabar were measured by the Surface Monitor system as well as laboratory-type XRD and micro-Raman techniques in this study. The patterns were analyzed and compared in order to generalize the experience for identifying cinnabar existing in different objects. The four samples tested were applied to simulating the cases of real cultural objects. The intention of the application study is to give advices to testers who are not quite familiar with the feature of cultural relic samples so that they can be experienced when they face more complicated samples and bad experimental conditions, or have to find the best testing method for a specific object. This study also gives mineralogists and museum conservators practical methods to learn the real composition of some unknown objects.

2 Materials and methods

2.1 Materials

Four samples (raw mineral, polished gemstone, pigment powder and Chinese ink stick) were measured in this study. The pigment powder sample was pressed into a thin tablet on a glass slide for holding the whole laser spots in portable coupled XRF-XRD and micro-Raman measurements, while other samples were measured without special preparation.

2.2 Portable coupled XRF-XRD measurement

The samples were measured using an Assing Surface Monitor XRF-XRD integrated system in situ. For XRF, the main parameters included step acquisition time (10 s), pre-heating time (0 s), tube angle (45°) and detector angle (45°); for XRD, the main parameters included working voltage (50 kV), tube current (75 μ A), XRD energy (9.71 keV, Au target), start angle (20°), stop angle (70°) and step angle (0.1°). The experiment scenes are shown in Figs. 1 and 2. The surface of the operation software is shown in Fig. 3.

2.3 Analysis of the portable XRF spectra

Once the portable coupled XRF-XRD measurement of a sample was finished, the XRF spectrum was analyzed first. Possible elements were selected manually at the XRF match surface by considering both the characteristic lines and the detected peaks. The elemental selection range is in principle from atomic number 11 (Na) to 100 (Fm) at the XRF match surface (see Fig. 4).

Fig. 1 Portable coupled XRF-XRD experiment scenes for the samples. **a** Raw mineral. **b** Polished gemstone. **c** Pigment powder. **d** Chinese ink stick. The left arm was the Newton Scientific Inc. Mini-X X-ray tube, the right arm was the Amptek X-123 SDD X-ray spectrometer, and the middle was the samples placed on glass slides. The polished gemstone was fixed at the plasticine to ensure the flat surface measured was parallel to the ground. The laser spot indicated the measurement position

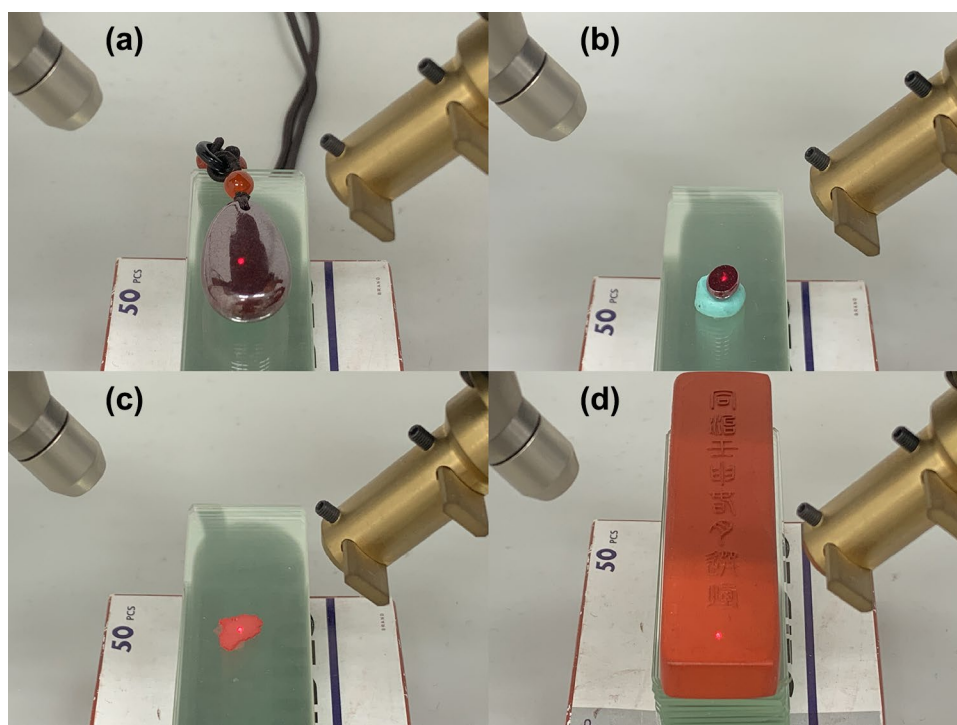


Fig. 2 The whole system including a controlling laptop (left), a removable apparatus (middle) and a multifunctional case (right)

2.4 Analysis of the portable XRD patterns

Once the analysis of XRF spectrum of a sample was done, analysis of its XRD pattern was performed. At the XRD free search surface “Mineral” was selected from the database options. The possible elements detected by XRF were selected from the periodic table (in green); the “AUTO” button can be used to automatically rule out the heavy elements and inert elements not present (in red); other

cells corresponded to light elements not detected or out of the application of XRF, and they can be selected, removed or left without operation according to the operator’s experience. The two options, either “At least one must be present” or “All must be present”, was selected based on the operator’s judgment as well (see Fig. 5). After these, the “SEARCH” button was clicked to enable the search for possible phases.

2.5 Laboratory-type XRD measurement and analysis of the patterns

Polished gemstone (0.885 g) and pigment powder (0.050 g) were also measured using a Bruker D8 ADVANCE poly-functional X-ray diffractometer (40 kV, 40 mA, Cu target) while the other two samples were not measured due to their unsuitable sizes. The patterns acquired were analyzed by using the Materials Data Inc. (MDI) Jade 5.0 software. The standard phase data were based on the built-in database ICDD PDF-2(2004).

2.6 Raman spectroscopy measurement and analysis of the spectra

The four samples were measured using a Renishaw inVia Reflex laser micro-Raman spectrometer *in situ*. The excitation wavelength employed included 532 nm, 633 nm and 785 nm. The instrument parameters were adjusted

Fig. 3 The initial surface of the operation software

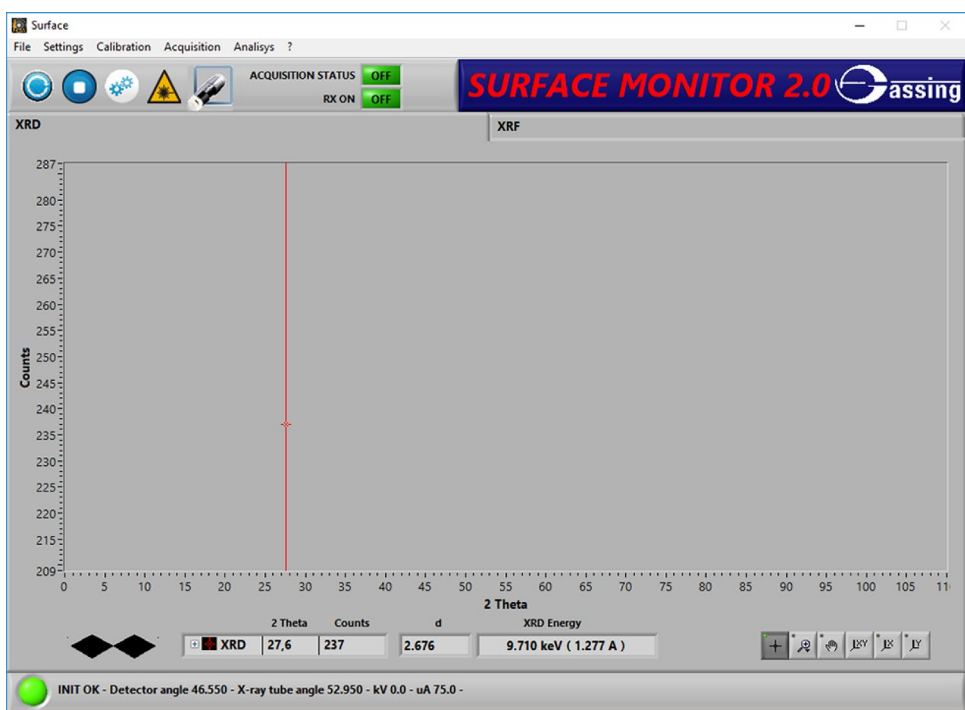
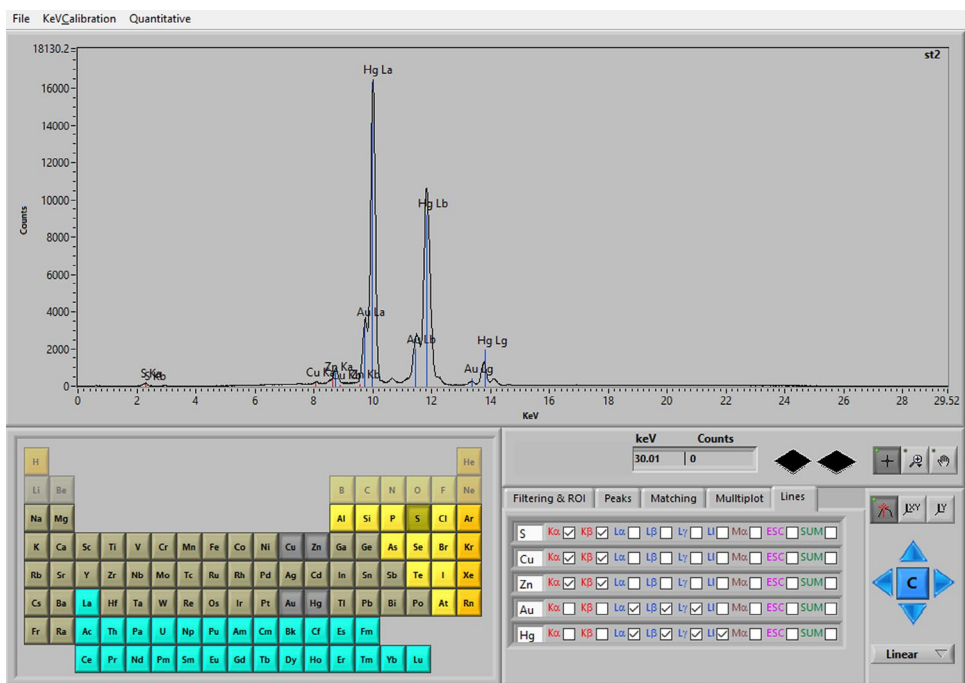


Fig. 4 The XRF match surface



according to the specific cases of each sample (see Table 1). The experiment scene is shown in Fig. 6. The spectra acquired were analyzed by seeking the relevant information from references.

Raw data obtained in portable coupled XRF-XRD, laboratory-type XRD and micro-Raman experiments are given in Electronic Supplementary Material 1 (ESM1).

3 Results and discussion

3.1 Portable coupled XRF-XRD results

It can be seen from Fig. 7 that Hg and S were commonly detected from raw mineral, polished gemstone and pigment powder samples, while the characteristic lines for

Fig. 5 The XRD free search surface

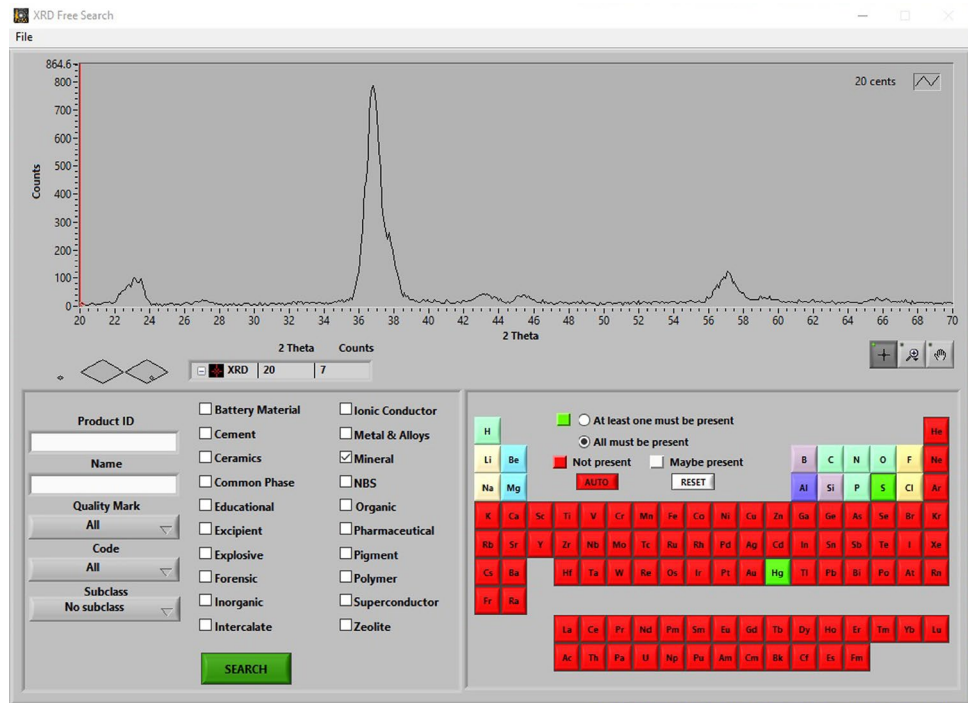


Table 1 Instrument parameters for different samples

Sample	Raw mineral	Polished gem	Pigment powder	Ink stick
Laser wavelength = 532 nm				
Time	1000 ms	1000 ms	1000 ms	1000 ms
Spot diameter	865 nm	865 nm	865 nm	865 nm
Power	1%	0.5%	1%	0.05%
Accumulations	32	32	32	12
Laser wavelength = 633 nm				
Time	1000 ms	1000 ms	1000 ms	1000 ms
Spot diameter	1030 nm	1030 nm	1030 nm	1030 nm
Power	1%	1%	1%	1%
Accumulations	12	12	1	202
Laser wavelength = 785 nm				
Time	1000 ms	1000 ms	1000 ms	10,000 ms
Spot diameter	1277 nm	1277 nm	1277 nm	1277 nm
Power	10%	5%	1%	10%
Accumulations	12	12	1	1

Au were originated from the Au anode. Ca and Fe were detected as trace elements from the pigment powder sample, which indicates additives or impurity substances in the pigment, while raw mineral and polished gemstone samples seem to be purely composed of Hg and S. The detection of S was more obvious in the raw mineral sample, but in general it was insignificant from the three samples, as the portable XRF is insensitive to the light elements in principle. On the other hand, Pb was detected as the primary element from the Chinese ink

stick sample, and S, Ca and Fe were also detected. The absence of Hg implies that the Chinese ink stick sample is unlikely to be composed of cinnabar. The detection of S, Ca and Fe was more obvious than from the other three samples, indicating that additives or impurity substances occupy a more significant position in the sample. Since Au was the anode material set in the portable system, the relative content of elements can also be compared roughly by calculating the ratios of peak intensity (different elements) to peak intensity (Au) (see Table 2). The



Fig. 6 Micro-Raman experiment scene for the raw mineral sample

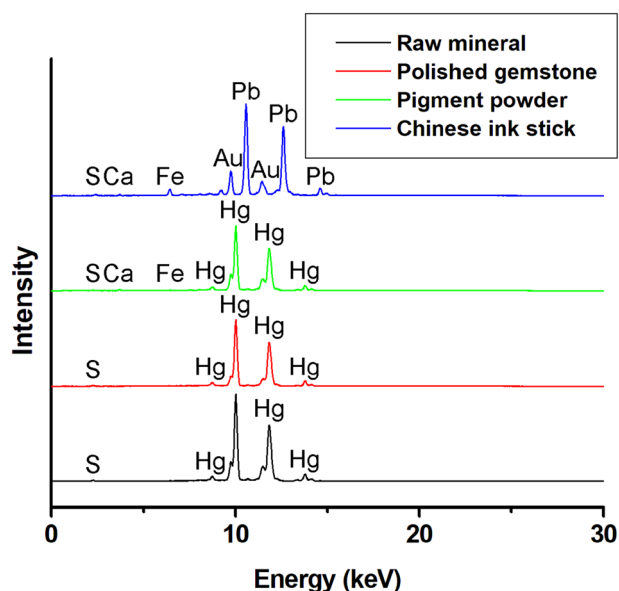


Fig. 7 Portable XRF spectra for the four samples

XRF results give a clear direction that element Hg (or Pb) should be considered primarily in the phase identification, and S should be regarded as the most likely non-metallic element.

Based on the above recognition, Hg and S were both selected as the elements present in raw mineral, polished gemstone and pigment powder samples. The system then showed that there were 59 possible phases in each case. Cinnabar was regarded as the most likely phase for the pigment powder sample by comparing the measured pattern with the characteristic lines. From Fig. 8c it can be seen that the major peaks fitted the lines well, which proves that cinnabar is the major component

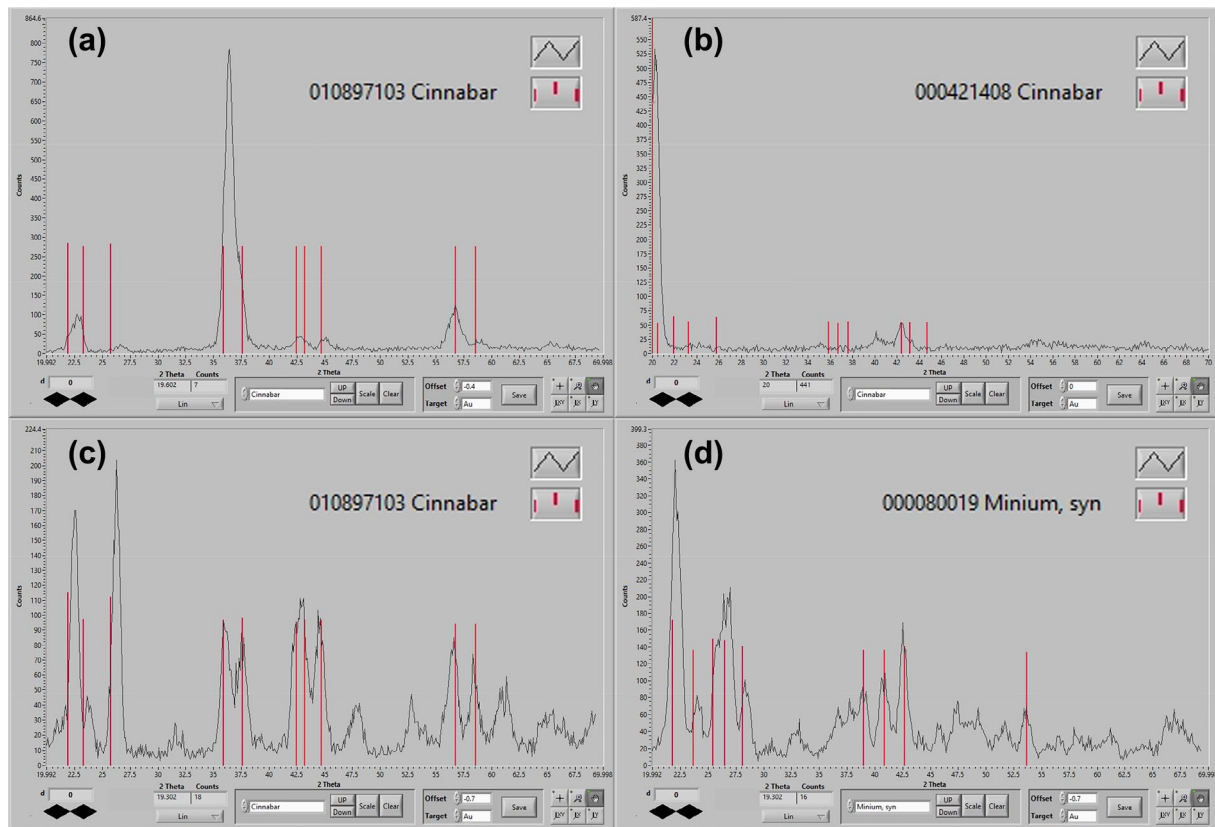
in the sample. However, there still remained some peaks which cannot be recognized by the system, which may be originated from the trace additives or impurity substances, or caused by the absence of some featured lines, as a defect of the software [15]. Raw mineral and polished gemstone samples were both regarded as mainly composed of cinnabar, but the pattern characteristics and the phases identified were different. The raw mineral featured an intense peak and several weak peaks on the pattern, and the peak positions fitted the standard lines in general (Fig. 8a), while the suspicious intense peak for the polished gemstone was located at a very low angle, and it was actually hard to definitely confirm the identification due to the preferential orientation [16] (Fig. 8b). On the other hand, Pb and S were both selected as the elements present in the Chinese ink stick sample, but the 95 possible phases given by the system actually did not fit the measured pattern, indicating that S probably exists in the trace additives or impurity substances. In this case, as the commonest element on the earth which just in principle cannot be detected by the portable XRF, O was considered. By selecting Pb and O simultaneously, 302 possible phases were found by the system automatically, among which minium (Pb_3O_4) was regarded as the most likely phase (Fig. 8d). The unmarked peaks may also be attributed to the software defect or trace additives or impurity substances. In general, it is practicable to identify the major phases of some pigments using the system, but the system is not sensitive enough to the trace phases. The presence of heavy elements is advantageous to the efficient identification, as the portable XRF is more sensitive to heavy elements. For minerals fully composed of light elements, it is necessary to further generalize experiences in choosing phase search strategies and simplifying the screening process. Moreover, since the measured position is indicated by a laser spot generated from the built-in interferometer, the measured surface must hold the whole laser spot (radius = 1 mm) to ensure accuracy and effectiveness of the working distance. Besides, the measured position must be thick enough to prevent penetration by X-ray beams. On the whole, only a tiny sample volume is needed in theory, while in this study it was determined by experiments that the volume of the cinnabar pigment powder needed is around 0.001 g.

3.2 Laboratory-type XRD results

Polished gemstone and pigment powder samples are both regarded as mainly composed of cinnabar (JCPDS 42–1408) by laboratory-type XRD (Fig. 9). It was found that the powder sample was reflected well by the pattern with various intense and weak peaks when it was measured

Table 2 Peak intensity counts obtained from portable XRF and peak intensity ratios calculated

Samples	Elements	Peak position (keV)	Intensity counts	Element/Au
Raw mineral	Au	9.71	3345	1.000
	S	2.31	184	0.055
	Hg	10.01	16,482	4.927
Polished gemstone	Au	9.71	1703	1.000
	S	2.31	116	0.068
	Hg	10.01	12,568	7.380
Pigment powder	Au	9.71	2853	1.000
	S	2.31	102	0.036
	Ca	3.69	200	0.070
	Fe	6.40	83	0.029
	Hg	10.01	12,296	4.310
Chinese ink stick	Au	9.71	4231	1.000
	S	2.31	84	0.020
	Ca	3.69	206	0.049
	Fe	6.40	1120	0.265
	Hg	10.01	271	0.064
	Pb	10.55	17,385	4.109

**Fig. 8** Portable XRD patterns. **a** Raw mineral. **b** Polished gemstone. **c** Pigment powder. **d** Chinese ink stick

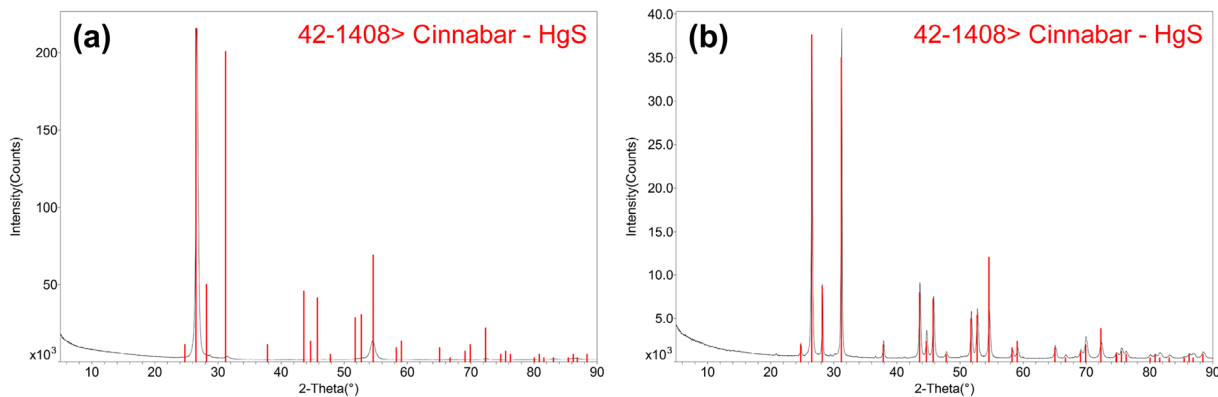


Fig. 9 Laboratory-type XRD patterns. **a** Polished gemstone. **b** Pigment powder

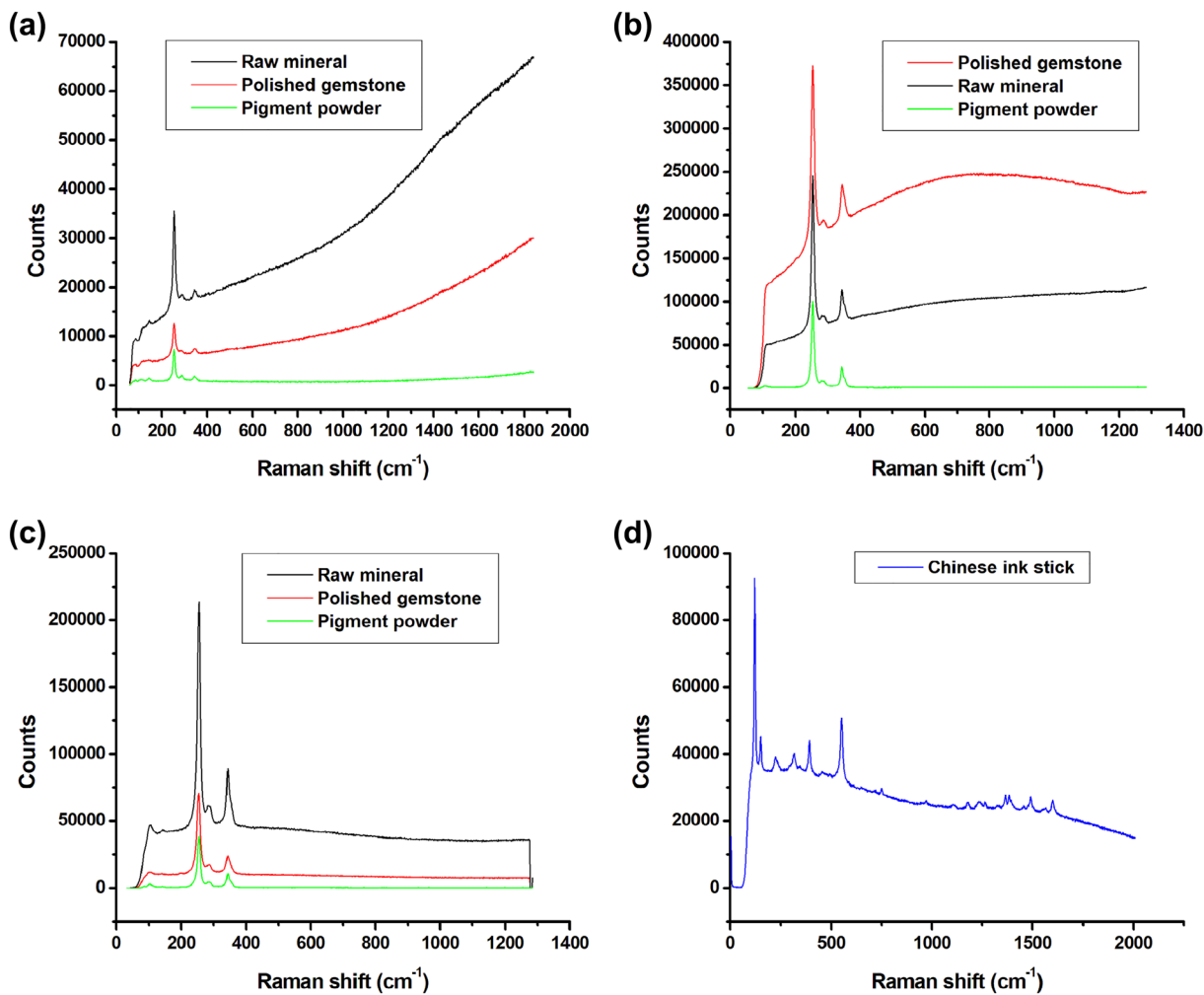


Fig. 10 Raman spectra. **a** Spectra for raw mineral, polished gemstone and pigment powder excited by 532 nm laser. **b** Spectra for raw mineral, polished gemstone and pigment powder excited by

633 nm laser. **c** Spectra for raw mineral, polished gemstone and pigment powder excited by 785 nm laser. **d** Spectrum for Chinese ink stick excited by 785 nm laser

using the portable integrated system, which was similar to that in the laboratory-type XRD case; raw mineral and Chinese ink stick samples were reflected by the portable XRD patterns with lower quality, while details of the polished gemstone sample showed by both methods were the fewest. The results indicate that the integrated system is more suitable to be applied to powder samples, while in some cases measuring bulk samples may lead to absence of pattern details.

3.3 Micro-Raman results

The Raman spectra obtained under the optimal parameters are shown in Fig. 10. The following characteristics were found in the spectra:

1. In the cases of 532 nm and 633 nm wavelength, the spectra for raw mineral and polished gemstone presented a baseline drift, while the spectra for pigment powder did not present an obvious baseline drift.
2. In the case of 785 nm wavelength, the spectra for raw mineral, polished gemstone and pigment powder did not present an obvious baseline drift.
3. For raw mineral, polished gemstone and pigment powder samples, the baseline drift in the case of 532 nm was the most significant, while less significant in the cases of 633 nm and 785 nm in proper order.
4. The spectra appearances for raw mineral, polished gemstone and pigment powder were similar in each case of excitation wavelength.
5. The significant peaks found for raw mineral, polished gemstone and pigment powder were similar in position in the three cases, as 253.9, 286.0 and 343.5 cm^{-1} on average (see Table 3).
6. The characteristic peaks for the Chinese ink stick sample were not excited by employing 532 nm wavelength but 633 nm and 785 nm wavelength (see Figs. 10 and 11).
7. For the Chinese ink stick sample, the baseline drift was more significant in the case of 633 nm than that of 785 nm wavelength, especially in the region lower than 1200 cm^{-1} .
8. The spectra for the Chinese ink stick sample were totally different from those for raw mineral, polished gemstone and pigment powder.
9. The significant peaks found for the Chinese ink stick sample were similar in position in the cases of 633 nm and 785 nm wavelength, as 120.3, 150.8, 225.8, 312.7, 390.7, 549.8, 748.0, 969.4, 1107.0, 1175.6, 1230.2,

Table 3 Peak positions (cm^{-1}) for different samples

Sample	Raw mineral	Polished gem	Pigment powder	Chinese ink stick
Peaks (532 nm)	253.8, 288.3, 343.7	253.8, 288.3, 343.7	253.8, 288.3, 343.7	no peak
Peaks (633 nm)	254.0, 285.1, 343.0	254.0, 287.7, 344.4	254.0, 282.5, 343.0	549.8, 747.2, 967.1, 1105.7, 1172.0, 1226.6, 1259.7, 1359.0, 1378.4, 1452.3, 1486.2, 1557.7, 1593.1
Peaks (785 nm)	254.3, 284.2, 343.4	253.0, 285.5, 343.4	254.3, 284.2, 343.4	120.3, 150.8, 225.8, 312.7, 390.7, 549.7, 748.7, 971.6, 1108.2, 1179.1, 1233.8, 1264.1, 1364.8, 1382.8, 1455.3, 1490.6, 1555.4, 1600.2

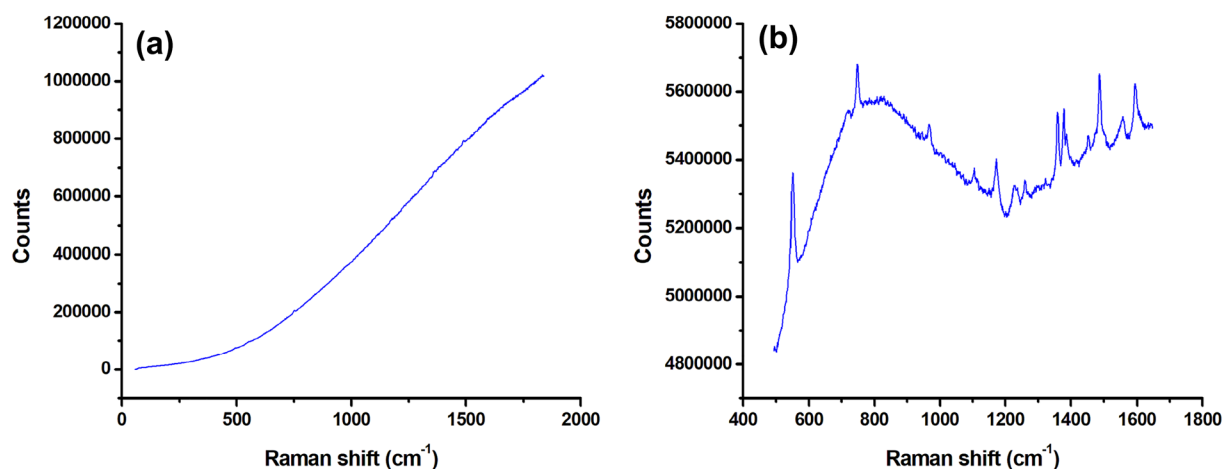


Fig. 11 Raman spectra for Chinese ink stick excited by **a** 532 nm laser and **b** 633 nm laser

1261.9, 1361.9, 1380.6, 1453.8, 1488.4, 1556.6 and 1596.7 cm^{-1} on average (see Table 3).

The authors made the corresponding explanations to the above phenomena:

1. The surface energy is accumulated rapidly when the material is irradiated by the laser, which may cause the Raman scattering effect, as well as fluorescence. The fluorescence spectrum features wide bands while looks like a curve of low slope when only a small region is measured, which is the origination of baseline drift in Raman spectra [17]. In other words, the baseline drift in fact reflects Raman spectra interfered by fluorescence [18, 19], which may significantly cover the key Raman signals sometimes. The results indicate that raw mineral and polished gemstone are sensitive to laser of 532 nm or 633 nm wavelength, while pigment powder is insensitive and thus little fluorescence is produced.
2. Raw mineral, polished gemstone and pigment powder were insensitive to laser of 785 nm wavelength, indicating that 785 nm is the best wavelength for measuring these three samples and getting the Raman spectra without significant fluorescence.
3. Based on the above results and discussion, it is clear that 785 nm is more suitable to be used as the excitation wavelength for the measurement of cinnabar.
4. Raw mineral, polished gemstone and pigment powder samples are almost identical in chemical composition.
5. The significant peaks found for raw mineral, polished gemstone and pigment powder are in accord with those for cinnabar reported in the references [20–23]. The peak centered at 253.9 cm^{-1} is attributed to the typical stretching vibration of Hg–S bond, while the peaks centered at 286.0 and 343.5 cm^{-1} are regarded as the transverse optical phonon signals of the semiconductor cinnabar [21, 24].
6. 633 nm and 785 nm are more suitable to be set as the laser wavelength for identifying the Chinese ink stick sample.
7. Fluorescence interference was very significant in the case of 633 nm, but 633 nm wavelength is useful for exciting the Raman signals in the region between 1000 and 1600 cm^{-1} . On the other hand, 785 nm wavelength is more suitable for acquiring the information included in the region between 100 and 1000 cm^{-1} . Thus, the two wavelength values were both adopted in order to obtain the full structural information about the Chinese ink stick sample.
8. The Chinese ink stick sample is different from raw mineral, polished gemstone and pigment powder in the

chemical composition. Namely, cinnabar is probably not the basic composition of the Chinese ink stick sample according to the Raman spectra.

9. The significant peaks centered at 120.3, 150.8, 225.8, 312.7, 390.7 and 549.8 cm^{-1} for the Chinese ink stick sample are in accord with those for minium reported in the references [20, 25–27]. The peaks in the region between 1000 and 1600 cm^{-1} are attributed to the following signals according to the literatures [28, 29]: 1175.6 cm^{-1} : C–N azo symmetric bending; 1230.2 cm^{-1} : phenyl-OH modes; 1261.9 cm^{-1} : C–C skeletal stretching; 1361.9 cm^{-1} : aromatic rings vibrations; 1380.6 cm^{-1} : N-phenyl stretching; 1453.8 cm^{-1} : N=N stretching; 1488.4 cm^{-1} : azo-benzene ring vibration; 1556.6 cm^{-1} : naphthalene ring stretching; 1596.7 cm^{-1} : aromatic quadrant stretching.

The above results indicate that cinnabar is the basic component of raw mineral, polished gemstone and pigment powder samples, while the Chinese ink stick sample is basically composed of minium (Pb_3O_4) instead of cinnabar, which are in accord with the portable coupled XRF-XRD results. Furthermore, the Raman bands in the region between 1000 and 1600 cm^{-1} indicate a characteristic signal of the azo dyes, which means the producer of the Chinese ink stick sample had added some red dyes to the minium powders to simulate the color of cinnabar.

3.4 Comparison of the three methods

Based on the above experiment process and results, it is clear that:

1. Less time is needed if micro-Raman is selected as the method to acquire a spectrum including enough structural information. However, the optimization of Raman instrument parameters is highly dependent on operators' experience, while the analysis of Raman spectra is based on the relevant information available in scattered literatures. Raman is thus regarded as a rapid non-destructive technique for identifying minerals like cinnabar, as well as a highly technological method including great challenges to users.
2. Portable coupled XRF-XRD has no advantage in measurement speed because only the step mode is available in the system. Currently, this technique is also inferior to laboratory-type XRD in the intelligence of result analysis because there is no automatic comparison and sort function for hundreds of possible phases found by the built-in software, increasing the workload, while users have to be very careful in order to reduce judgment error.
3. With mature instrument, software and database, laboratory-type XRD is the most reliable technique for

Table 4 Comparison of laboratory-type XRD, portable coupled XRF-XRD and micro-Raman techniques

Instrument type	Laboratory-type XRD	Portable coupled XRF-XRD	Micro-Raman
Instrument model	Bruker D8 Advance	Assing Surface Monitor 2.0	Renishaw inVia Reflex
Detection target	Phase	Element, phase	Group
Measurement area	cm level	mm level	µm level
Measurement speed	Fast	XRF: very fast; XRF-XRD: slow	Very fast
Analysis strategy	Comparing results with standard cards automatically	Comparing results with standard cards manually	Searching literatures for the relevant information available
Analysis difficulty	Easy	XRF: easy; XRD: hard	Hard
Database development	Developed	Developed	Developing
Method sensitivity	Low	XRF: high; XRD: low	High
Result reliability	Good	Good	Good
Typical applications in cultural heritage field	Ordinary inorganic powders or small objects; patinas	Inorganic pigments on oil paintings; gems; minerals; porcelains	Pigments; organic dyes; patinas; gems; precious objects
Main disadvantages	Unfit for large precious objects; low sensitivity to trace phases	Unfit for samples without flat surfaces; low pattern quality; software defects	Weak signals; incomplete database; high requirement for operator's experience

material identification among the three, but it is not quite suitable for the cultural heritage field mainly due to the sample preparation, the limitation of sample size and its low sensitivity to trace phases.

- Both portable coupled XRF-XRD and micro-Raman are promising techniques in the cultural heritage field because of their non-destructive feature. Micro-Raman shows less limitation of sample size, which widens its application to more samples, especially irregularly-shaped objects, big objects or traces of samples. The improvement of method and the integration of database are the main directions of the development of micro-Raman. By contrast, portable coupled XRF-XRD is less suitable for the measurement of the above samples. Both its hardware and software have a large space to improve.

Main characteristics of the three techniques are compared and listed in Table 4.

Cultural objects are quite different from common samples in several aspects. Compared with samples which can be reproduced by modern techniques, cultural objects are unique, which not only means their preciousness, but also indicates irregularity and complexity in identification. The uniqueness of cultural objects is reflected physically by the variety of size and chemically by the variety of composition. In many cases museum conservators have to face the difficulty of identifying big objects made from multiple components. Typical examples include oil paintings made of canvas (or board) and mineral pigments, Chinese paintings made of paper, mineral pigments and vegetable dyes, ancient bronzes made from copper, tin, lead and certain trace elements, Chinese porcelains composed of various minerals and pigments, etc. Portable coupled XRF-XRD

and micro-Raman are useful for the identification of cinnabar according to the present study, but weak points still remain. It is still hard to learn the exact composition of the trace phases by both methods in this study, indicating that in real cases of measuring cultural objects the minor components may not be exactly identified as well. On the other hand, real cultural objects of various sizes and materials certainly bring more challenges. Wider application of both techniques in the cultural heritage field calls for hardware improvements, software updates, more real application cases and more user experiences.

4 Conclusions

The Assing Surface Monitor XRF-XRD integrated system is useful for identifying a mass of cinnabar existing in powders and bulk materials. Samples must have a flat surface large enough to hold the whole laser spot (radius = 1 mm) to ensure accuracy and effectiveness of the measurement. The sample volume needed can be as low as 0.001 g if the sample is mainly composed of cinnabar. Pigments with similar color, such as minium, can be easily distinguished from cinnabar by using the system. The presence of heavy elements favors the identification of possible phases in the software. The system has a great potential to be more widely applied to cultural heritage conservation and other fields such as mineralogy and material science for the non-destructive identification of major phases in the samples. Hardware and software of the system, and the phase search strategy, leave much room to improve. The micro-Raman technique is superior to the XRF-XRD integrated system in application range, measurement period, method sensitivity and pattern resolution. Samples

composed of cinnabar, other minerals, organic additives, or other impurities, can be identified by the highly-sensitive micro-Raman technique provided that the relation between peak position and group information is available. Further development and integration of Raman databases are key to the improvement of Raman applications.

Acknowledgements This work was financially supported by Shanghai Museum Research Project. The authors sincerely acknowledge Shanghai Jiao Tong University Instrumental Analysis Center for providing help on laboratory-type XRD characterization.

Author contributions Jingyi Shen designed the whole project, conducted portable coupled XRF-XRD and laboratory-type XRD experiments, wrote and revised the whole manuscript; Yijia Shen conducted micro-Raman spectroscopy measurements. Both authors read and approved the manuscript.

Funding This work was financially supported by Shanghai Museum Research Project.

Availability of data and material All data generated or analyzed during this study are included in the article and its supplementary information files.

Declarations

Conflict of interest The authors declare that there is no conflict of interest.

Consent for publication Corresponding Author signs for and accepts responsibility for releasing this article on behalf of any and all Co-Authors.

Open Access This article is licensed under a Creative Commons Attribution 4.0 International License, which permits use, sharing, adaptation, distribution and reproduction in any medium or format, as long as you give appropriate credit to the original author(s) and the source, provide a link to the Creative Commons licence, and indicate if changes were made. The images or other third party material in this article are included in the article's Creative Commons licence, unless indicated otherwise in a credit line to the material. If material is not included in the article's Creative Commons licence and your intended use is not permitted by statutory regulation or exceeds the permitted use, you will need to obtain permission directly from the copyright holder. To view a copy of this licence, visit <http://creativecommons.org/licenses/by/4.0/>.

References

1. Bonewitz RL (2008) Rocks and minerals. Dorling Kindersley, London
2. Evans JW, De Jonghe LC (2016) High-temperature processes for the production of metals and glass. The production and processing of inorganic materials. Springer, Cham, pp 241–280
3. Duan L, Guo L, Wang L, Yin Q, Zhang C, Zheng Y, Liu E (2018) Application of metabolomics in toxicity evaluation of traditional Chinese medicines. *Chin Med* 13:60. <https://doi.org/10.1186/s13020-018-0218-5>
4. Neiman MK, Balonis M, Kakoulli I (2015) Cinnabar alteration in archaeological wall paintings: an experimental and theoretical approach. *Appl Phys A* 121:915–938. <https://doi.org/10.1007/s00339-015-9456-x>
5. Wang J, Wang J (1999) Application of vermilion pigments in ancient China. *Sci Conserv Archaeol* 11:40–45 (in Chinese)
6. Nakai I, Abe Y (2012) Portable X-ray powder diffractometer for the analysis of art and archaeological materials. *Appl Phys A* 106:279–293. <https://doi.org/10.1007/s00339-011-6694-4>
7. Romano FP, Pappalardo G, Pappalardo L, Rizzo F (2006) The new version of the portable XRD system of the LANDIS laboratory and its application for the non-destructive characterisation of pigments in ancient Roman frescoes. *Nuovo Cimento B* 121:881–885. <https://doi.org/10.1393/ncb/i2007-10020-9>
8. Van de Voorde L, Van Pevénage J, De Langhe K, De Wolf R, Vekemans B, Vincze L, Vandenabeele P, Martens MPJ (2014) Non-destructive in situ study of “Mad Meg” by Pieter Bruegel the elder using mobile x-ray fluorescence, x-ray diffraction and Raman spectrometers. *Spectrochim Acta B* 97:1–6. <https://doi.org/10.1016/j.sab.2014.04.006>
9. Bersani D, Lottici PP (2010) Applications of Raman spectroscopy to gemology. *Anal Bioanal Chem* 397:2631–2646. <https://doi.org/10.1007/s00216-010-3700-1>
10. Dele-Dubois ML, Dhamelincoeur P, Poirot JP, Schubnel HJ (1986) Differentiation between gems and synthetic minerals by laser Raman microspectroscopy. *J Mol Struct* 143:135–138. [https://doi.org/10.1016/0022-2860\(86\)85222-X](https://doi.org/10.1016/0022-2860(86)85222-X)
11. Chen D, Xie X, Ao H, Liu J, Peng C (2017) Raman spectroscopy in quality control of Chinese herbal medicine. *J Chin Med Assoc* 80:288–296. <https://doi.org/10.1016/j.jcma.2016.11.009>
12. Bicchieri M, Monti M, Piantanida G, Pinzari F, Sodo A (2011) Non-destructive spectroscopic characterization of parchment documents. *Vib Spectrosc* 55:267–272. <https://doi.org/10.1016/j.vibspec.2010.12.006>
13. Grammatikakis I, Demadis KD, Kyriakidis E, Cabeza A, Leon-Reina L (2017) New evidence about the use of serpentinite in the Minoan architecture. A μ -Raman based study of the “House of the High Priest” drain in Knossos. *J Archaeol Sci Rep* 16:316–321. <https://doi.org/10.1016/j.jasrep.2017.09.029>
14. Tomasini E, Palamarczuk V, Zalduendo MM, Halac EB, López JMP, Fuertes MC (2020) The colors of San José pottery from Yocavil valley Argentine Northwest Strategy for the characterization of archaeological pigments using non-destructive techniques. *J Archaeol Sci Rep* 29:102123. <https://doi.org/10.1016/j.jasrep.2019.102123>
15. Shen J (2020) Nondestructive identification of gemstones by using a portable XRF-XRD system: an illuminating study for expanding its application in museums. *SN Appl Sci* 2:372. <https://doi.org/10.1007/s42452-020-2183-8>
16. Zhang G, Zhang Q (1992) Preliminary study of gems and jades identification with x-ray diffraction technique. *Hunan Geol* 11:315–317 (in Chinese)
17. Lv M (2017) Baseline correction and noise suppression of Raman spectroscopy. Dissertation, University of Electronic Science and Technology of China (in Chinese)
18. Tan H, Brown SD (2002) Wavelet analysis applied to removing non-constant, varying spectroscopic background in multivariate calibration. *Chemometr* 16:228–240. <https://doi.org/10.1002/cem.717>
19. Zhang X, Chen S, Wu B, Yang G, Xu F (2016) Adaptive method for denoising Raman spectral imaging data and its applications to spectral analysis in plant cell walls. *Chin J Anal Chem* 44:1846–1851. <https://doi.org/10.11895/j.issn.0253-3820.160392> (in Chinese)
20. Burgio L, Clark RJH (2001) Library of FT-Raman spectra of pigments, minerals, pigment media and varnishes, and

- supplement to existing library of Raman spectra of pigments with visible excitation. *Spectrochim Acta A* 57:1491–1521. [https://doi.org/10.1016/s1386-1425\(00\)00495-9](https://doi.org/10.1016/s1386-1425(00)00495-9)
21. Chang J, Zhang W, Xu S, Xuan X, Su B, Xu W (2010) Raman spectra of the pigments in ancient wall paintings. *Spectrosc Spectr Anal* 30:277–278 **(in Chinese)**
 22. Sun Y, Jiang K, Zhang N (2019) Pigment analysis of Lotus Cave statues using Raman spectroscopy and microscopy. *Sci Conserv Archaeol* 31:77–85. <https://doi.org/10.16334/j.cnki.cn31-1652/k.2019.02.011> **(in Chinese)**
 23. Wang X, Wang C, Yang J, Chen L, Feng J, Shi M (2004) Analysis of wall-painting pigments in Fenghui Tomb using HREM and Raman spectroscopy. *J Instrum Anal* 23:1–4 **(in Chinese)**
 24. Gotoshia SV, Gotoshia LV (2008) Laser Raman and resonance Raman spectroscopies of natural semiconductor mineral cinnabar, α -HgS, from various mines. *J Phys D Appl Phys* 41:115406. <https://doi.org/10.1088/0022-3727/41/11/115406>
 25. Si Y, Jiang H, Wang B, He Q, Hu Y, Yang Y, Wang C (2013) Raman microspectroscopic analysis of polychrome wooden artifact from the Astana Tomb of the Tang Dynasty Xinjiang China. *Spectrosc Spectr Anal* 33:2607–2611 **(in Chinese)**
 26. Wang Y, Zhang X, Wu N (2015) Raman analysis of the painted sculptures pigments of Wuhou Temple in Chengdu. *J Light Scatt* 27:355–358. <https://doi.org/10.13883/j.issn1004-5929.201504009> **(in Chinese)**
 27. Wang Y (2018) Analysis and study of the Tangka of Xixia Thousand Buddha Niches. *J Light Scatt* 30:150–155. <https://doi.org/10.13883/j.issn1004-5929.201802010> **(in Chinese)**
 28. Cesaratto A, Centeno SA, Lombardi JR, Shibayama N, Leona M (2017) A complete Raman study of common acid red dyes: application to the identification of artistic materials in polychrome prints. *J Raman Spectrosc* 48:601–609. <https://doi.org/10.1002/jrs.5082>
 29. Lv J, Liu S, Li Y, Feng J, Liu Y, Zhou S (2015) Differentiation of inks used for seals by confocal Raman microscopy and Fourier transform infrared microscopy. *Spectrosc* 30:36–43

Publisher's Note Springer Nature remains neutral with regard to jurisdictional claims in published maps and institutional affiliations.